ChemPubSoc Europe

DOI: 10.1002/cphc.201200927

Bare Clusters Derived from Protein Templates: Au_{25}^+, Au_{38}^+ and Au_{102}^+

Ananya Baksi,[a] Thalappil Pradeep,*[a] Bokwon Yoon,[b] Constantine Yannouleas,[b] and Uzi Landman*[b]

A discrete sequence of bare gold clusters of well-defined nuclearity, namely Au_{25}^+, Au_{38}^+ and Au_{102}^+, formed in a process that starts from gold-bound adducts of the protein lysozyme, were detected in the gas phase. It is proposed that subsequent to laser desorption ionization, gold clusters form in the gas phase, with the protein serving as a confining growth environment that provides an effective reservoir for dissipation of the cluster aggregation and stabilization energy. First-principles calculations reveal that the growing gold clusters can be electronically stabilized in the protein environment, achieving electronic closed-shell structures as a result of bonding interactions with the protein. Calculations for a cluster with 38 gold atoms reveal that gold interaction with the protein results in breaking of the disulfide bonds of the cystine units, and that the binding of the cysteine residues to the cluster depletes the number of delocalized electrons in the cluster, resulting in opening of a super-atom electronic gap. This shell-closure stabilization mechanism confers enhanced stability to the gold clusters. Once formed as stable magic number aggregates in the protein growth medium, the gold clusters become detached from the protein template and are observed as bare Au_n^+ ($n = 25$, 38, and 102) clusters.

1. Introduction

Clusters of noble metals, particularly gold, with precise nuclearity (number of atoms) and overall molecular composition continue to be a topic of intense experimental and theoretical research endeavors. These efforts aim at understanding the basic factors, such as electronic structure, atomic packing, and adsorbed layers that underlie the appearance of certain structural motifs and control the size evolution, which bridges the cluster-size domain with the bulk condensed phase. These studies are also motivated by certain properties exhibited by clusters, such as high chemical reactivity, catalytic activity and intense luminescence, which may be exploited in future technologies.[1] While the structures of bare, as well as protected (passivated), gold clusters have been studied for close to two decades,[2] research activities on ligated analogues have intensified significantly in recent years[3–5] and crystal structures of four of them, namely, $Au_{25}(SR)_{18}$,[3e,f] $Au_{36}(SR)_{24}$,[3k] $Au_{38}(SR)_{24}$,[4e] and $Au_{102}(SR)_{44}$[5a] (SR, alkyl thiolate ligand derived from RSH) have been solved using X-ray crystallography total structure determination, meaning determination of the atomic positions of both the core and surface atoms.

Clusters protected with proteins[6] have been a rather recent addition to this family of materials, with the clusters exhibiting stable luminescence and the proteins retaining their biological activity[6e] and biocompatibility. Certain clusters, for example, Au_{13}, Au_{25}, Au_{38} and some others, have been proposed to exist within protein templates. Mass spectrometry is an indispensible tool for investigations of clusters, particularly since precise measurement of molecular composition is possible with soft ionization methodologies such as laser desorption. However, laser desorption and ionization often result in fragmentation of the S–C bond on the cluster core, resulting in Au_nS_m aggregates. To date, formation of bare gas-phase Au_n clusters, especially those with structural and electronic stability, has not been observed in studies of metal cluster complexes with proteins.

Cluster aggregation and growth from precursors via the assembly of atoms or molecules, is accompanied by energy release and efficient removal of the aggregation and stabilization energy, which is often achieved through collisional cooling and is a prerequisite for stable cluster growth. Typically laser desorption is followed by equilibration of the plasma in an inert gas leading to the formation of clusters. This has been eminently demonstrated in the case of fullerenes.[7] We considered the possibility of forming stable clusters of gold using protein templates as an energy relaxation medium—a heat-bath reservoir—during cluster growth.

In this paper, we show experimentally, through mass spectrometry, and theoretically, using first-principles quantum calculations, that formation of stable gas-phase clusters with spe-

[a] A. Baksi, Prof. Dr. T. Pradeep
DST Unit of Nanoscience (DST UNS)
Department of Chemistry
Indian Institute of Technology Madras
Chennai 600036 (India)
E-mail: pradeep@iitm.ac.in

[b] Dr. B. Yoon, Dr. C. Yannouleas, Prof. Dr. U. Landman
School of Physics
Georgia Institute of Technology
Atlanta, GA 30332-0430 (USA)
E-mail: uzi.landman@physics.gatech.edu

Supporting information for this article is available on the WWW under http://dx.doi.org/10.1002/cphc.201200927.

WILEY ONLINE LIBRARY © 2013 Wiley-VCH Verlag GmbH & Co. KGaA, Weinheim

cific nuclearities (that is, a discrete sequence of cluster sizes characterized by enhanced stability compared to other sizes) can be achieved through the use of biomolecules, in particular, proteins. Here, the proteins act as selective cluster nucleation templates offering spatially confining protective growth volumes and electronic stabilization of the aggregating metal clusters. In addition, the proteins serve as effective reservoirs for the removal of cluster formation and stabilization energy. The results shown herein constitute the first observation of protein-template-derived stable gas-phase clusters of formulae Au_{18}, Au_{25}, Au_{38} and Au_{102}, although their ligand protected analogues have been known for some time. Most of our studies used lysozyme, from chicken egg white (Lyz) as a model protein because of its relatively light mass, which allows the acquisition of high-quality mass spectra in the monomer and oligomer regions. Associated studies have also been conducted with bovine serum albumin (BSA) and native lactoferrin (NLf).

The paper is organized as follows. In the Experimental Section (at the end of the manuscript) we describe the experimental and theoretical methodologies. In Section 2 we present and discuss our experimental (2.1–2.4) and theoretical (2.5) results. We summarize our results in Section 3, and put them in perspective in the light of current and future investigations.

2. Results and Discussion

2.1. Observation of Size-Selected Bare Gold Clusters

A discrete sequence of bare gold clusters of well-defined nuclearities, Au_{25}^{+}, Au_{38}^{+} and Au_{102}^{+} were created in a process of laser desorption, which starts from gold-bound precursor adducts (Lyz–Au) of the protein, Lyz. The adducts were made by incubating $HAuCl_4{\cdot}3H_2O$ with Lyz at room temperature (30 °C) at various concentrations (see the Experimental Section). In the Lyz–Au adducts, gold exist in the +1 form as seen from X-ray photoelectron spectroscopy (XPS) in the Au4f region[6g] and the reduction (Au^{3+} to Au^{1+}) is proposed to occur by amino acids and/or by the oxidation of the cystine disulfide bonds in the protein[11] (Section 2.5). Luminescent gold clusters in protein templates are formed from these adducts upon exposing the system to an alkaline medium.[6g] The Lyz–Au adducts observed by us here, however, are not luminescent in the visible spectral window. Several macromolecules such as DNA are known to produce noble metal clusters although reduction typically uses external reducing agents.[8a] Protein-protected clusters generally invoke the mechanism of tryptophan-induced reduction.[8b] For this study, we prepared the Au^{1+} state in the solution phase and conducted laser desorption on this material in the solid state.

The protein used in this study, lysozyme, has 129 amino acids, including eight cysteine residues, $-SCH_2CH(NH_2)CO_2H$. These cysteine residues form four disulfide bonds, thus making four cystines, located between positions 6–127, 30–115, 64–80 and 76–94. As we show below, our theoretical simulations predicted, and experiments confirm[6i] that interaction with gold results in splitting of the cystine disulfide bonds. For the parent protein, matrix-assisted laser desorption ionization mass spectrometric (MALDI-MS) analysis shows a series of peaks in the positive ion spectrum corresponding to Lyz^{+} (*m/z* 14,363) and its oligomers such as Lyz_2^{+} (*m/z* ~28810), Lyz_3^{+} (*m/z* ~43300), and so forth, along with Lyz^{2+} (*m/z* 7180), with uncertainty increasing with an increase in the mass number. Except for the Lyz^{2+} feature, the mass spectrum of the parent Lyz does not show any signal in the *m/z* range of 3000–9000 (Figure 2, bottom-most trace). However, spectra of the Lyz–Au adduct present a completely different picture where distinctly different peaks are seen. These features keep increasing in intensity as a function of the Au^{3+} concentration used to make the adduct. An examination of the mass spectrum shows that the new peaks are mostly spaced at *m/z* 197, due to Au. The maxima of the peaks correspond to $Au_{18}S_4^{+}$, Au_{25}^{+} and Au_{38}^{+} with a separation due to Au on either side of the maxima (Figure 1, note the regions marked a, b and c). While the ions in the Au_{25} region are composed solely of gold, the Au_{18} region shows ions with some sulfur additions, in the form of $Au_{18+n}S_{4+m}^{+}$. We conjecture here that these sulfur additions are the result of interaction of Au with the protein medium in which the metal cluster ions are formed. This is supported by the predictions of our first-principles calculations (see below) and experimental measurements[6i] (see also Figure S5, Supporting Information). In the Au_{18}^{+} region, sulfur attachment is

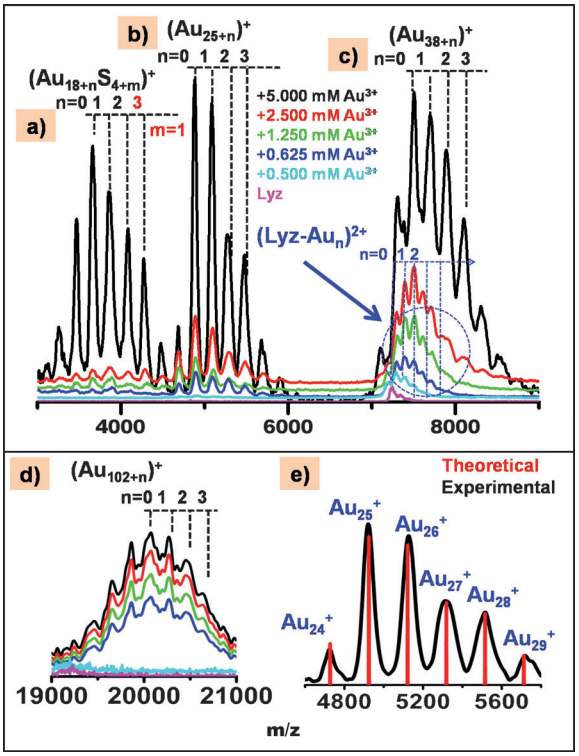

Figure 1. MALDI-MS of Lyz–Au adduct in the linear positive mode showing distinct features of Au clusters. The spectrum of parent Lyz is also shown. The bare cluster series seen are separately shown: a) $Au_{18}S_4$, b) Au_{25} and c) Au_{38} and d) Au_{102}. The peaks show a separation of *m/z* 197. The circled region of (c) shows a Au uptake of Lyz^{2+} with a separation due to the Au^{2+} series. In (e) the experimental spectrum in the Au_{25} region is compared with the calculated peak positions (in red). Colors of the traces correspond to the Au^{3+} concentration used, which are indicated.

© 2013 Wiley-VCH Verlag GmbH & Co. KGaA, Weinheim

again evidenced by additional mass increase in the Au_{20}^{+} mass, where the peak corresponds to $Au_{20}S_5^{+}$. The series of bare clusters are labeled such that the highest-intensity peak is marked as $n=0$. Peaks above and below $n=0$ imply that clusters of relatively poor stability are also formed. It is noteworthy that while different ions are seen in the spectrum around the Au_{18}^{+} and Au_{25}^{+} regions, the $Au_{18}S_4^{+}$ and Au_{25}^{+} species themselves are highest in intensity.

The Au_{38}^{+} region overlaps with Lyz^{2+} and its Au pick-up peaks (see below), but the latter are much weaker in intensity at the highest Au^{3+} concentration used. At this concentration, the mass spectrum is spaced at $m/z=197$, due to gold, while for $(Lyz–Au_n)^{2+}$, the peaks are separated by 99. The nearly 100 Da mass difference (between Au^{2+} and Au^{1+}) is easy to be resolved at this mass range by the instrument.

Upon further examination of the mass spectrum, other ions such as Au_{102}^{+} are also observable. In this mass region (Figure 1 d), the clusters appear in the spectrum above a gold concentration of 0.625 mM and there was no ion signal of significance below this concentration regime. In this range, adjacent cores are nearly equally stable as intensity difference is not too high between the peaks. The mass assignments are accurate as a comparison of the experimental and theoretical mass numbers in the Au_{25}^{+} region would indicate (Figure 1 e). For the other regions, experimental and theoretical peak positions are compared in Figure S1.

Lysozyme is a rather small protein and in solution it is unlikely to accommodate gold clusters of 25, 38 or 102 atoms in a single molecule. Indeed as we discuss in section 2.2, a Lyz molecule is found to attach only up to ~10 Au atoms. Consequently, we propose that reactions in the plasma generated after laser ionization/desorption to underlie the formation of the detected gold clusters. Upon laser irradiation, a gaseous plasma is created, composed of ions and neutrals of gold atoms and aggregates, protein molecules, and Lyz–Au adducts, as well as electrons. We also note here that gaseous Lyz–Au adducts are likely to be conformationally modified compared to the solution phase. These plasma constituents interact to form larger aggregates (as known in the case of plasma desorption). Such reactions may include the following reaction schemes (and cascades thereof) [Eqs. (1)–(3)]:

$$\mathrm{Au}_n + \mathrm{Au}_m{}^{+} \rightarrow \mathrm{Au}_{n+m}{}^{+}, \qquad \mathrm{Au}_n + \mathrm{Au}_m \rightarrow \mathrm{Au}_{n+m} \quad n,m = 1,2,3,\ldots, \tag{1}$$

$$[\mathrm{Lyz} - \mathrm{Au}_m]^{+} + \mathrm{Au}_n \rightarrow [\mathrm{Lyz} - \mathrm{Au}_{m+n}]^{+} \quad m = 0,1,2,\ldots; n = 1,2,3\ldots, \tag{2}$$

$$[\mathrm{Lyz} - \mathrm{Au}_n]^{+} + \mathrm{Lyz} - \mathrm{Au}_m \rightarrow [\mathrm{Lyz} - \mathrm{Au}_{n+k}]^{+} + \mathrm{Lyz} - \mathrm{Au}_{m-k} \quad n,m = 1,2,3,.; k\ (\leq m) = 1,2,\ldots, \tag{3}$$

where Equation (3) describes metals transfer between two Lyz–Au adducts. As discussed by us below (Section 2.5), in the Lyz–Au_n adduct, the gold cluster is anchored to the protein through binding to the cysteine residues resulting from barrierless cleavage by gold of the cystine disulfide bond with four cystine groups per lysozyme molecule. The disulfide bond cleavage is accompanied by changes in the protein molecular conformation (Sections 2.5 and S5). We note here that Au_n^{+} (with $n=1, 2, 3,\ldots$) species are seen in the laser desorption mass spectrum of Au salts. These occur due to photoreduction and reactions of the type described in Equation (1). Larger aggregates by the extension of the same process occur here because of the delayed extraction (used in MALDI-MS) of the ions. In our experiments, the ions (and neutrals) formed are extracted only after a finite delay time of 1200 ns to allow the desorbed species in the gaseous plasma to interact (see description of the MALDI-MS method in the Experimental Section). The plasma reactions between low-energy ions and neutrals have a number of precedents. For example, we note here observation of $C_{(60+n)}^{+}$ in secondary ion mass spectrometry (SIMS)[9] of C_{60} films (due to gas-phase reactions between C_{60}^{+} and C_2 species, derived by fragmentation of C_{60}). In our case, the above reactions are further facilitated by the abundance of protein molecules (and their gold-cluster adducts) in the (plasma) reaction zone, since their relatively large mass slows down their movement and separation from the plasma cloud. Relaxation of the metal cluster aggregation energy (binding and excess vibrational energies) is facilitated by coupling of the growing metal cluster to the large number of degrees of freedom of the host protein molecule. As gold clusters evolve following the above growth processes, certain cluster nuclearities, that is selected cluster sizes (number of gold atoms) of enhanced stability are formed (for the electronic stabilization mechanism of "magic number" cluster sizes, see Section 2.5), and they eventually detach from the lysozyme template, and get detected as bare gold cluster cations.

2.2. Au Uptake by Lyz—Observations in the Solid State

The bare clusters are formed from Au–protein adducts, which are seen in the integral form in the MALDI MS spectra. As mentioned before, the positive ion spectrum of Lyz displays features due to Lyz^{+} and its oligomers along with Lyz^{2+} (Figure 2, bottom-most trace). For Au^{1+}–Lyz, these peaks are shifted to higher masses. For the Lyz^{+} peak, the maximum intense feature showed a mass shift of about 600 Da from the parent Lyz, due to Au pick-up. Upon closer examination, multiple peaks are seen, starting from parent lysozyme peaks and each one of the peaks is separated by m/z 197 due to Au. A maximum of nine Au additions were seen for Lyz^{+}, with reduced intensity (this region is expanded in inset a). Gold uptake is also exhibited by Lyz_2^{+} giving $(Lyz_2–Au_n)^{+}$ (inset b). The larger Lyz aggregates (Lyz_3^{+}, Lyz_4^{+},…) also take up gold, as shown in Figure 2, but the resolution is not adequate to see individual Au uptakes clearly at Lyz_3^{+} and beyond. The number of Au uptake peaks increases with increase in Au^{3+} concentration (spectra at varying Au^{3+} concentrations are shown in Figure 2) and the intensity of free protein without any Au attachment decreases simultaneously. Thus we conclude that up to ~10 Au attachments are possible in Lyz–Au_n adducts. In any case, at the concentrations used (maximum molar ratios of 1:3 for Lyz:Au), it is unlikely that in solution (and thus in a solid made from that solution) a protein molecule would pick up a much larger

© 2013 Wiley-VCH Verlag GmbH & Co. KGaA, Weinheim

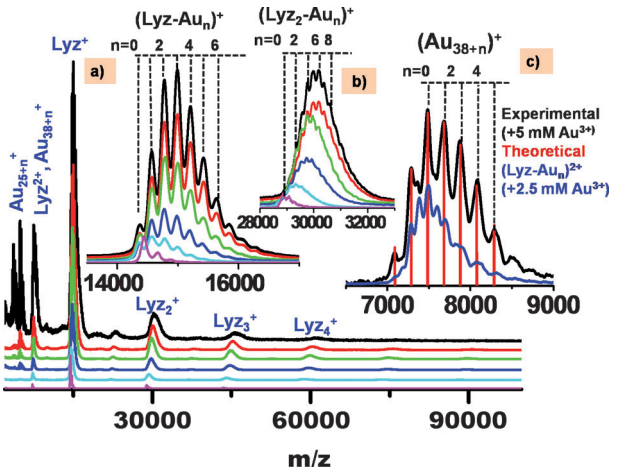

Figure 2. MALDI-MS spectrum of as-synthesized Lyz–Au adduct in the linear positive ion mode at various concentrations of Au^{3+} used for incubation. The spectrum shows Au attachment, seen at the various peaks derived from Lyz such as the monomer (Lyz), dimer (Lyz_2), trimer (Lyz_3), and so forth. Expanded views show multiple Au attachment to a) Lyz and b) Lyz_2^+. In (c) theoretical (red) and experimental (black) values for Au_{38}^+ region along with Au uptake by Lyz^{2+} are compared. In these traces (c), two Au^{3+} concentrations are used: 5 mM (black) and 2.5 mM (blue) because of their good intensity. All the colors used are the same as those mentioned in Figure 1.

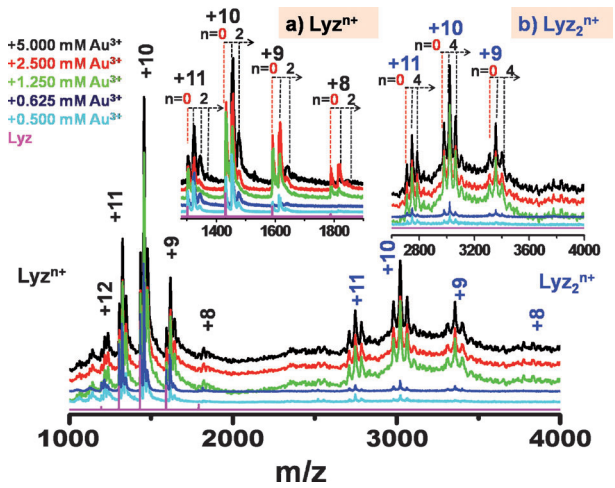

Figure 3. ESI-MS spectrum of Lyz–Au adduct in the positive-ion mode, in the region of *m/z* 500–4000. The peaks observed are due to Au uptake by Lyz at different charge states. Peak separation is corresponding to the Au uptake by that specific charge state. Insets: a) peaks of the Lyz^{n+} series and b) the same for the Lyz_2^{n+} series.

number of gold atoms (e.g. 25, 38 or 102), although aggregates of protein–gold adducts may have such numbers of gold atoms.

The attachment of gold to the lysozyme molecule is likely due to the cystine residues, which act as protecting thiolates and upon reaction with Au^{3+}, the latter is converted to Au^+.[10] The lower mass region of the spectrum shows the bare clusters, shown in Figure 1. As the $(Lyz–Au_n)^{2+}$ peaks overlap with the Au_{38+n}^+ region, we have confirmed the authenticity of the assignments by comparing the spectrum with the calculated masses of Au_{38+n}^+ (Figure 2, inset c) where we can see that some of the peaks due to $(Lyz–Au_n)^{2+}$ are distinctly different.

2.3. Study of the Solution State

To explore whether the gold clusters form in the solution, we undertook an electrospray ionization mass spectrometry (ESI-MS) study of the Lyz–Au adducts. Lysozyme gives well-defined mass spectra and good charge distribution. The +10 charge is the most stable in the case of both the monomer and the dimer in the spectral range studied. From the ESI-MS studies (Figure 3), it is evident that Au is picked up by the protein at all the concentrations studied. Here, larger relative intensities are found for the Au-added peaks with an increase in the Au^{3+} concentration. The separation due to multiple Au atom pick-ups can be also seen at high concentration of Au^{3+}, especially in the dimer region (these are marked in the inset). Both the Lyz monomer and dimer show maximum intensities corresponding to the +10 charge state, implying that this state is the most stable, as in the protein mass spectrum. The separation between the main protein peak and the gold uptake peaks changes with the charge state: the separation is 19.7 for +10 charge while it is 21.9 for +9 and 24.6 for +8. In these spectra, a limited number of Au uptakes is seen, unlike in the MALDI-MS data where up to nine Au additions are seen. This is probably due to the increased Columbic repulsion of multiply charged states as in 10+ and consequent loss of the metal ion to increase the stability. From the ESI-MS data, we conclude that the bare gold clusters observed in the MALDI mass spectrum (Figure 1 and 2) do not form in the solution phase.

2.4. Dependence on Other Factors

Several control experiments were performed and the important ones are presented below:

1) To prove that the chemistry seen is independent of the photon flux, a laser-intensity-dependent study was performed. MALDI-MS did not show significant laser intensity dependence, although the Au_n^+ peaks were enhanced with increasing intensity (Figure S2). No new features were seen at higher intensity. In the Au_{18}^+ region one continues to observe the aforementioned $Au_{18+n}S_{4+m}^+$ features (Figure 1a) even at higher laser intensities, indicating the absence of Au–S bond breakage. These results are important as typically at increased laser intensity, fragmentation occurs, especially when the linkages are weaker as in the case of ligand protection of a metal core.
2) Several proteins known to make luminescent clusters in solution[6] were probed to make bare clusters. The data (Figure S3) suggest that while lysozyme is most efficient in cluster formation, others such as bovine serum albumin (BSA) and NLf also make clusters. The parent proteins do not show any peaks in this mass range.
3) While clusters form in both the positive- and negative-ion modes, cluster formation was more efficient in the former (Figure 4), as typically negative ions are 500 times weaker than the corresponding positive ion signals. No new fea-

© 2013 Wiley-VCH Verlag GmbH & Co. KGaA, Weinheim

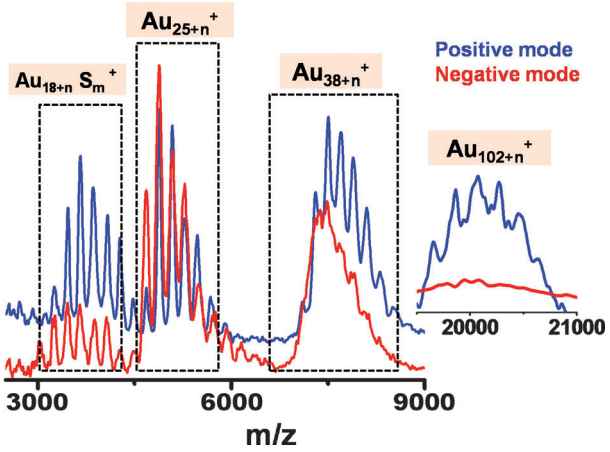

Figure 4. Positive (blue) and negative (red) MALDI-MS spectra of the Lyz–Au adduct in the linear mode at a concentration of 5 mM Au^{3+} as all the peaks are coming with good intensity at this concentration. In the negative mode the intensity is 500 times less than in the positive mode and therefore the spectra above have been scaled suitably.

tures were seen in the negative mode. In the negative mode the Au_{38}^{+} and Au_{102}^{+} regions are not well-resolved. From this study, it is confirmed that the as-prepared bare clusters are more stable in the cationic form. Therefore, all other studies were carried out in the linear positive mode.

4) The precursor solution was investigated over time to see any time dependent changes occur in MALDI-MS (Figure S4). There was no change in the peak positions in the Au_{18}^{+} and Au_{25}^{+} region, only the intensity was increased. The enhanced intensity may be due to the availability of more Au^{+} ions with time as more Au^{3+} is expected to be consumed to become Au^{+}. In the Au_{38}^{+} region, the spectra show a somewhat more pronounced dependence on the solution incubation time than for the other sizes (Au_{18}^{+}, Au_{25}^{+} and Au_{102}^{+} regions). Just after mixing Au^{3+} with the lysozyme, the peaks do not appear properly. However, $(Lyz–Au_n)^{2+}$ peaks that overlap with the Au_{38}^{+} came up. After two hours from mixing, the peaks began to appear, but not with sufficient intensity. After four hours of reaction, peaks in the Au_{38}^{+} region started to become prominent. But after six hours, the intensity increased significantly and kept getting higher, and by twelve hours, became comparable to the intensity of the Au_{25}^{+} region. It is pertinent to note here that it has been reported that in the solution phase, upon passage of time, Au_{25} becomes the only prominent cluster among a mixture of clusters.[3j] The larger mass-spectrometrically-measured abundance of Au_n^{+} ($n \leq 38$) bare clusters indicates that it is harder to accommodate and sustain the growth of larger clusters (e.g. $n = 102$) in the lysozyme template. This is most likely because the protein's relatively small size restricts (conformationally) the size of the forming gold cluster. The above-noted somewhat larger sensitivity of the Au_{38}^{+} cluster to the solution incubation time, may arise because of specific structural characteristics of certain solution Lyz–gold adducts (with up to about ten gold atoms per lysozyme molecule) that (kinetically) require more time to form, and that subsequent to laser ionization and desorption (Section 2.1) react favorably to form this size cluster. Overall, we conclude that the above observations further supports our conclusions about the role of the protein molecules in the cluster formation process, acting as a gold storage medium, enabling the nucleation, growth and stabilization (see below) of gold clusters.

2.5. Theoretical Studies

Since the mechanisms and dynamics of the cluster growth processes are not amenable for investigation with mass spectrometry, these aspects are outside the scope of this paper. Instead we focus on experimental identification and characterization of the products of the interaction between gold and protein molecules, and on theoretical exploration of certain size-dependent stabilization mechanisms mediated by the interaction of the formed gold clusters with the protein growth medium. In particular, in our theoretical discussion, we focus on binding of the gold clusters to the cysteine residues that result from dissociative interaction of the clusters with the dimeric amino acid, cystine, of the lysozyme molecule.

As aforementioned, cluster formation must be accompanied by efficient dissipation of the heat of aggregation by the growth medium. Macromolecules, in general, and proteins in particular, are characterized by a vast number of degrees of freedom, covering a broad energy (frequency) range. Consequently, it is likely that vibrational motions and (local) conformational changes of the host protein molecules would facilitate efficient removal of the heat generated in the process of gold cluster nucleation and growth. We postulate that the observed growth of metal clusters in the protein environment involves formation of protein-bound metal cluster nuclei whose growth is facilitated by dissipation, annealing and equilibration processes. Furthermore, in this picture, the specific chemistry of the protein template and its interaction with the gold clusters play an important role in (electronic) stabilization of certain self-selecting "magic" sizes. The rest of this section is devoted to investigations of the electronic factors governing such cluster stabilization processes.

Of particular interest is the mass spectrometric measurement pertaining to the formation of a discrete, limited-in-number, series of metal clusters that punctuates the sequence of integers—specifically, gold cation clusters with 25, 38 and 102 atoms (Figure 1). This size-sequence of bare gold clusters is particularly interesting since it is the same as that found earlier for thiolate-protected gold clusters. However, in the latter case, the clusters are protected by a large number of ligands, that is, $Au_{25}(SR)_{18}$,[3e,f] $Au_{38}(SR)_{24}$,[4e] and $Au_{102}(SR)_{44}$[5a] (see also earlier findings in refs. [2b,c]), while in the present case the number of accessible thiols is limited by the number of cystines in the lysozyme molecule. We tacitly assume that because of steric effects (crowding), a given gold aggregate may simultaneously interact (i.e. form an adduct complex) with just a small number of lysozyme molecules, through formation of

© 2013 Wiley-VCH Verlag GmbH & Co. KGaA, Weinheim

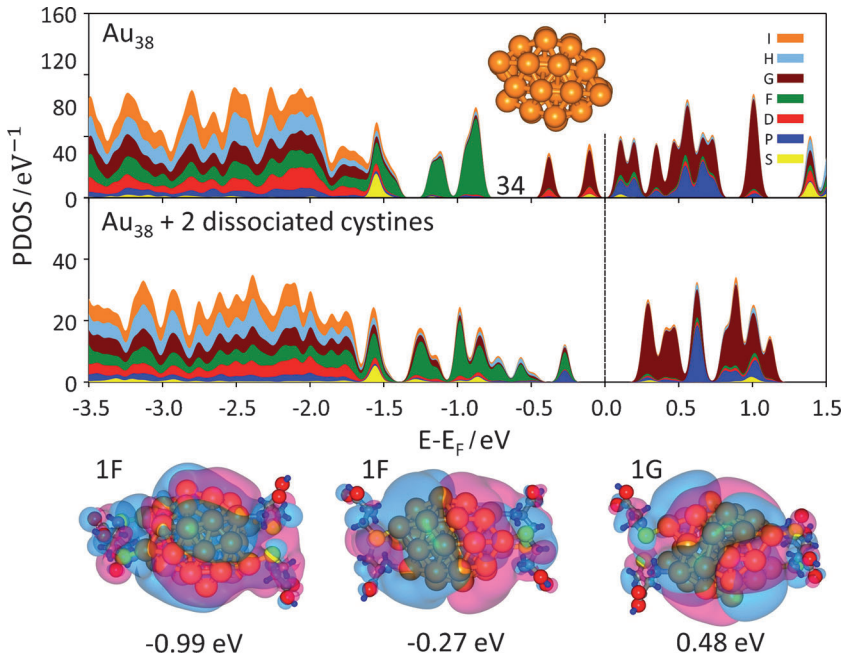

Figure 5. PDOS calculated for an optimized neutral bare Au_{38} cluster (upper panel), with an optimized deformed truncated octahedral, d-TO, structure, shown as an inset, whose energy is lower by 1.07 eV than that of the ideal TO isomer. Also shown is the PDOS for an optimized Au_{38}(cyteine)$_4$ cluster (bottom panel, with the optimized structure shown in Figure 6). The four adsorbed cysteine residues resulted from dissociation of the disulfide bonds in two adsorbed cystine molecules. Also shown for the cluster in the bottom panel are KS orbital images of two of the 1F orbitals near the top of the occupied spectrum (the one with $E-E_F=-0.27$ being the HOMO orbital), and of one of the unoccupied 1G orbitals. The weights of the angular momentum components of the displayed KS orbitals are given in S6. Dashed vertical line at $E-E_F=0$ denotes the location of the midpoint between the HOMO and the LUMO levels. In the orbital isosurface images, positive and negative orbital values are colored light blue and pink, and the orbital energies and symmetries (with the color key given on the right in the upper PDOS panel) are marked. The stabilization (shell closure gap) in the PDOS shown in the bottom panel is 0.54 eV.

gold–sulfur bonds. Indeed we observed gold attachment mainly to Lyz^+ and Lyz_n^+ ($n=2$–4) (see MALDI mass spectra in Figure 2, and related text).

As noted above, our discussion pertaining to the stabilization mechanism of the observed bare clusters (with $n=25$, 38, and 102 gold atoms), focuses on the interaction of the clusters with the thiol groups of the cysteine residues, which form as a result of the dissociative binding of cystine units of lysozyme to the forming clusters. In Figure 5 we display the calculated projected density of states (PDOS) (see the Methods Section), for an optimized (minimum energy) bare Au_{38} cluster (upper panel) and for the optimized structure of Au_{38}(cysteine)$_4$ (lower panel). While cystine is part of the lysozyme protein, we have considered here for simplicity its dissociative adsorption to the metal cluster as a free molecule. An optimal (minimum energy) atomic configuration of the four cysteine residues adsorbed on the Au_{38} cluster is shown in Figure 6. In Figure 5, as well as in the following ones, a vertical dashed line at $E-E_F=0$ denotes the location of the midpoint between the Kohn–Sham (KS) eigen-energies of the highest occupied molecular orbital (HOMO) and the lowest unoccupied one (LUMO).

In the following, we make use of the early proposal[2 g] where a "partial jellium" (PJ) model (used often in recent theoretical work on passivated metal clusters to explain "magic number" stability)[11] was first introduced for the analysis of the electronic structure of gold clusters. In agreement with the PJ model we find that while for a wide range of energies (located at the middle of the energy spectrum) the electronic wavefunctions (KS orbitals) exhibit localized character (associated with the atomic 5d electrons), the orbitals of states with energies near the top or bottom of the spectra are of delocalized (super-atom, jellium-like) character, derived from the atomic 6s electrons (see representative orbital images in Figures 5, 7 and 8). These delocalized states can be assigned particular symmetries [determined with the use of an expansion of the calculated wavefunction in spherical harmonics (see the Methods Section and Figure S5)], following the electronic cluster–shell model (CSM), with a (superatom) aufbau rule : $1S^2|1P^6|1D^{10}|2S^2|1F^{14}|2P^61G^{18}|2D^{10}3S^21H^{22}|2F^1$….where S, P, D, F, G, H, and I, correspond, respectively, to angular momenta, $l=0$, 1, 2, 3, 4, 5, and 6. We note here certain possible alterations in level ordering, for example, exchanging the locations of the $1D^{10}$ and $2S^2$ and of $3S^2$ and $1H^{22}$ levels, caused mainly by deviations of the cluster shape from spherical symmetry. In the above CSM scheme, the vertical lines denote shell-closures, with each

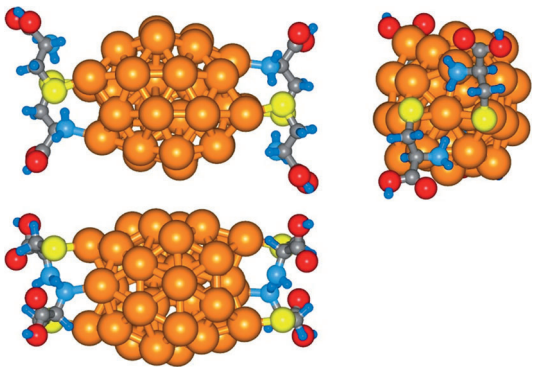

Figure 6. Three views of the structure of Au_{38} (cyteine)$_4$ (gold atoms represented by orange spheres) with four adsorbed cysteine [$HO_2CCH(NH_2)CH_2S$–] residues, resulting from two dissociated cystine units. Sulfur atoms are represented by yellow spheres, oxygen atoms by red spheres, carbons by gray spheres, nitrogen by larger light blue spheres, and hydrogen atoms by small dark blue spheres. The S–S distances, between two neighboring adsorbed cysteine residues, are d(S–S) = 4.50 Å and 4.42 Å, and the average S–Au bond length is 2.36 Å. For an undissociatively adsorbed cystine molecule d(S–S) = 2.21 Å and d(Au–S) = 2.545 Å and 2.495 Å.

© 2013 Wiley-VCH Verlag GmbH & Co. KGaA, Weinheim

closure accompanied by the opening of a stabilizing energy gap. Consequently, closed-shell clusters (that is, where the HOMO state of the cluster closes a shell) possess enhanced stability, and are termed "magic number" (MN) clusters. Such (spherical-like) clusters are comprised of $n^*=2$, 8, 18 (20), 34 (40), 58, 92, … delocalized electrons. In certain cases gaps may also occur at the magic numbers given in parenthesis (depending on the degree of deviation of the cluster structure from spherical symmetry, see for example, Figure 8(B) below).

We observe that for the neutral bare Au_{38} cluster (Figure 5 upper panel), $E-E_F=0$ falls within a dense band of states, that is, with no opening of a stabilization gap. We also note that a gap of 0.48 eV (denoted by the number 34 at the top panel of Figure 5) separates the peaks corresponding to the occupied 1F orbitals (colored green) from the two peaks (occupied by 4e) corresponding to 1G orbitals (colored brown, at the top of the spectrum in Figure 5, upper panel). This 34-electron superatom gap is the result of a $1S^2|1P^6|1D^{10}|2S^2|1F^{14}$ shell closure associated with the population of 17 delocalized orbitals (corresponding to double occupancy by 34 electrons). By itself, the Au_{38} cluster is not a "magic cluster", having an excess of four delocalized electrons (occupying the aforementioned two 1G states) and exhibiting merely a gap $\Delta_{HL}=0.21$ eV between the highest occupied (HOMO) and the lowest unoccupied (LUMO) molecular orbitals. However, we conjecture that the interaction of gold clusters with cystine units of the lysozyme template (four cystines in a lysozyme molecule derived from chicken egg white used in our experiment) may confer enhanced stability of the cluster by transforming it to a magic one. This conjecture is strongly supported by the results shown in Figure 5.

To assess the energetics of the above stabilization mechanism involving interaction of the gold clusters with the protein, we explored the binding of the Au_{38} cluster to the cystine molecules, $(SCH_2CH(NH_2)CO_2H)_2$. As before, for simplicity we consider free cystine molecules, while as part of the lysozyme they are bonded to the protein. A cystine molecule binds to the d-TO 38 atom gold cluster with an energy of 0.58 eV. This adsorption does not have a noticeable effect on the atomic arrangement, electronic structure and stability of the cluster. However, upon dissociation of the cystine molecule on the cluster (a process that entails a very small energy barrier), the two cysteine units (thiolate parts of the dimeric aminoacid, cystine) adsorb strongly to the cluster with a binding energy of 1.97 eV per cystine. Thus, when dissociatively adsorbing two cystine molecules (Figure 6) we get $E[Au_{38}(\text{d-TO})]+2E[\text{cystine})]-E[Au_{38}\ (\text{cysteine})_4]=3.94$ eV, where $E[X]$ denotes the total energy of the species X. The dissociative binding of two cystine molecules to the Au_{38} cluster (see Figure 6) is found to have a profound effect on the electronic structure of the cluster, with the sulfur–gold bonds engaging the four 1G electrons (corresponding to the two occupied peaks, colored brown, near $E-E_F=0$ in the upper panel of Figure 5), and, most importantly, opening a shell-closure stabilization gap $\Delta_{HL}=0.48$ eV (see lower panel, Figure 5). The KS orbital images of two of the 1F delocalized orbitals near the top of the occupied spectrum (the one with $E-E_F=-0.27$ eV being the HOMO orbital), and an image of the unoccupied 1G orbital (see bottom of Figure 5) confirm the above 34-electron superatom electronic shell structure. The above validates our conjecture pertaining to the shell-closure stabilization caused by the interaction of certain gold clusters (particularly Au_n with n close to a magic number, n^*) with the protein template.

The above first-principles calculations predict that the interaction of gold clusters with cystine residues of the lysozyme molecule would result in cleavage of the S–S bonds. This in turn may lead to change in the secondary structure of the protein. Such change is indeed seen in circular dichroism (CD) studies of protein-protected luminescent gold clusters in solution as well as in the IR spectrum of the same material in the solid state.[6i] Cleavage of S–S bonds has been found to lead to changes in the protein secondary structure (see Figure S5). We have shown that 28% of the α-helix structure is lost due to gold-cluster formation. Here we note that most of the cystine residues are in the α-helix region. Therefore S–S bond breakage directly affects the helical structure of the protein. Corresponding changes are also seen in an infrared spectroscopic study. Certain changes are observable also in the amide region (Figure S5). The variations in the α-helix region are better observable in the second derivative of the spectra (Figure S5). Such studies were performed as well on lactoferrin-protected luminescent gold clusters.[6f]

Further evidence for the interaction of the gold clusters with the sulfur-containing residues (cystines) in the lysozyme molecule can be obtained from measurements of XPS spectra. The Au–Cys interaction has a covalent component. Indeed, distinct features are observed in XPS measurements of protein–gold adducts, in the S (2p) and Au (4f) regions, supporting the covalent attachment of Au to the cysteines. The measured S (2p) signal is thiolate-like,[6g–i] supporting the disulfide bond cleavage. However, no corresponding change is seen in the N(1s) region upon the addition of gold to the lysozyme, indicating that formation of lysozyme–gold adducts does not involve bonding of gold to the amide region in the protein.

In Figures 7 and 8 we display the calculated PDOS for Au_{102}^+ (Figure 7) and for Au_{38}^+ and Au_{25}^+ (Figure 8). Such results were obtained for several structural isomers (with optimal cluster structures shown as an inset in Figures 7 and 8). We observe that as in the case of the neutral bare Au_{38} cluster (Figure 5 upper panel) for all the clusters considered here, $E-E_F=0$ falls within a dense band of states, that is, with no opening of a stabilization gap. The key observation is that while Au_n^+, with $n=102$, 38 and 25, are not magic-number clusters, the number of (delocalized) 6s electrons in each of these clusters is rather close to a magic number, that is $n^*=92$, 34, and 20, respectively. Consequently, these clusters may achieve magic-number stabilization even when the depletion in the number of delocalized electrons in the cluster is relatively small (through electronic interaction of the cluster with the protein). Specifically, for the clusters considered by us here (i.e. with $n=102$, 38 and 25), such stabilization through depletion of the number of delocalized electrons entails a rather small number of electrons, that is $n-n^*=10$, 4, and 5 electrons, respectively. As demonstrated by us above for the case of the

© 2013 Wiley-VCH Verlag GmbH & Co. KGaA, Weinheim

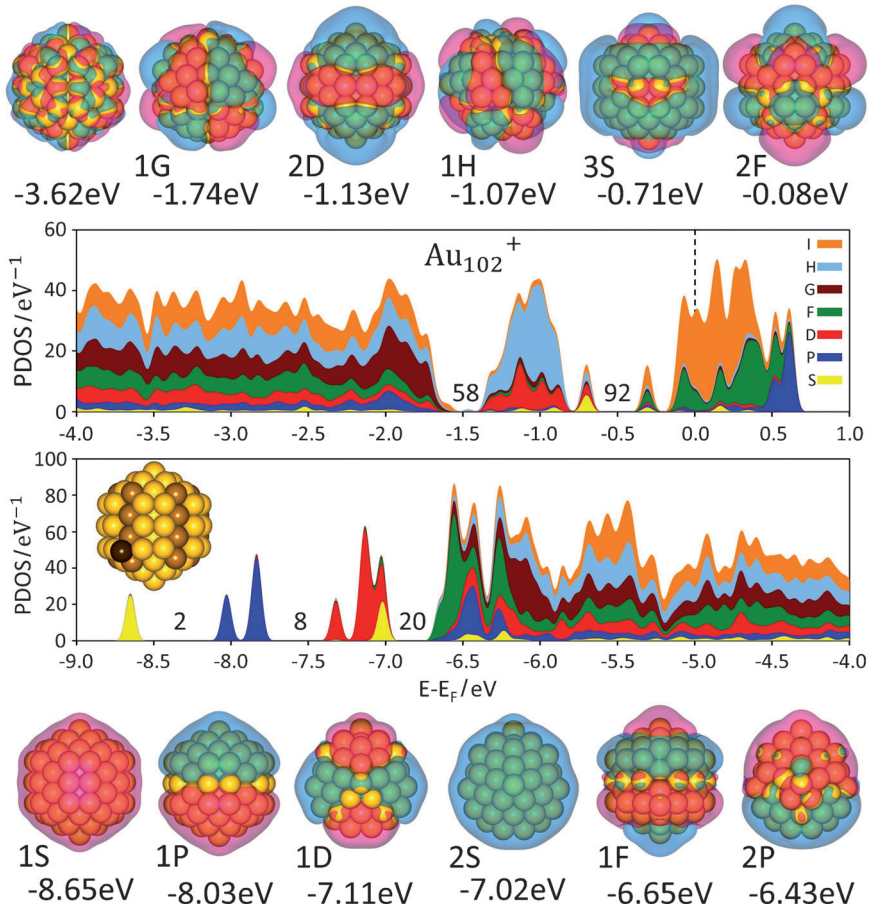

Figure 7. PDOS and KS orbital images calculated for an optimized Marks-decahedral (m-Dh) structure (left inset in bottom panel of the PDOS, with the gold atoms in the m-Dh "grooves" colored brown) of a Au_{102}^{+} cluster; the ideal m-Dh structure is comprised of 101 atoms, the extra atom in the Au_{102}^{+} cluster is positioned in the groove (see the extra atom, colored in darker brown, at the bottom left of the cluster structure shown in the inset). In the orbital isosurface images, positive and negative orbital values are colored light blue and pink, and the orbital energies and symmetries (with the color key given on the right in the upper PDOS panel) are marked. All orbitals shown are of delocalized character except the one at −3.62 eV (left in the upper panel) which corresponds to a localized orbital with atomic d character. The weights of the angular momentum components of the displayed KS orbitals are given in Figure S5. The number of electrons in delocalized orbitals (2, 8, 20, 58, and 92) corresponding to closed shells are marked in the shell-closure gaps. Note in particular the shell closure at $n^{*}=92$ obtained by depletion (10 electrons) of the number of delocalized electrons resulting from the interaction of the cluster with the protein environment and subsequent single ionization. The cluster is characterized by a spin projection $s_z={}^{1}/_{2}$.

Au_{38} cluster, such stabilization can occur in the lysozyme template through interactions of the aggregated gold cluster with cystine units of the protein, resulting in breaking of the disulfide bonds and strong binding of the cysteine residues to the cluster (while maintaining their peptide bond linkage to the protein). Once formed as stable magic-number clusters (anchored to the protein), release of the clusters from the protein template and ionization (in the gas phase) brings them to a cationic state Au_n^{+}, $n=102$, 38, and 25. We remark here that the cluster geometries that we describe here differ from those found in the case of the aforementioned thiol-passivated gold clusters,[3–5] since the latter clusters are protected by a large number of strongly interacting adsorbed molecules, whereas in the present case, during the formation process, the interaction between the clusters and the growth environment is of limited nature (only four disulfide groups in a Lyz molecule).

It is proposed that during laser desorption ionization of a protein–Au salt adduct, gold clusters form, with the protein serving as a confining cluster growth environment, providing an effective reservoir for dissipation of the aggregation and stabilization energy of the clusters. Furthemore, the first-principles calculations suggest that electronic interaction between the aggregating metal clusters and the lysozyme molecule (via the sulfur-containing cystine residues) stabilizes specific cluster sizes, at, or in the neighborhood of, electronic magic numbers. Clusters with these magic number sizes form a discrete size sequence with enhanced stability. Specifically, we demonstrate, with the use of results obtained from extensive first-principles calculations, that two cystine units dissociate upon interaction with Au_{38} (see Figure 6). The resulting four cysteine residues engage some of the delocalized electrons of the gold cluster (originating from the $6s^1$ electrons of the gold atoms), thus

Moreover, ultimately, as observed in the mass spectrum, the gold clusters appear bare (i.e. without the stabilizing ligands). We recall here that for the smallest observed gold cluster ions (around $n=18$), some sulfur addition, in the form of $Au_{18+n}S_{4+m}^{+}$ clusters, have been detected (see Figure 1), providing further evidence for the interaction between the gold clusters and the cystine units of the lysozyme prior to release of the clusters to the gas phase. Why the smaller clusters (containing a number of atoms centered on 18) are found to carry some small number of residual sulfur atoms, while the larger clusters (Au_n^{+}, $n=25$, 38, 102) appear bare, remains a topic for future research.

3. Conclusions

We reported here the results of a joint experimental (MALDI and electrospray ionization mass spectrometry) and theoretical (large-scale first-principles DFT electronic structure calculations) investigations pertaining to the formation of a discrete sequence of bare gold clusters of well-defined nuclearity, that is, Au_{25}^{+}, Au_{38}^{+} and Au_{102}^{+}, in the gas phase, by a novel process involving gold-bound complexes of the protein lysozyme.

© 2013 Wiley-VCH Verlag GmbH & Co. KGaA, Weinheim

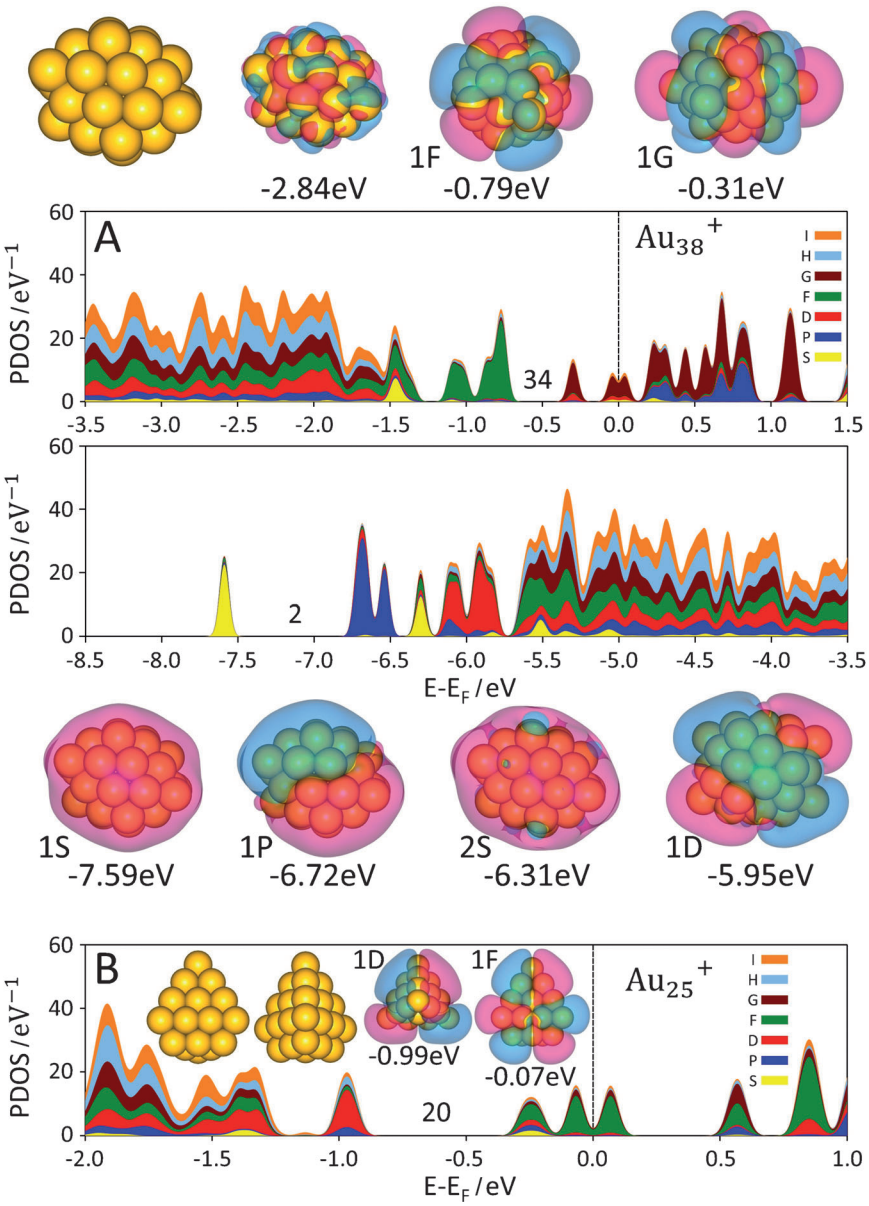

Figure 8. PDOS and KS orbital images calculated for: A) an optimized truncated octahedral (TO) structure (left image in the upper row) of a Au_{38}^{+} cluster, and B) an optimized tetrahedral-like structure (atomic structure images of the cluster, viewed from the front and back sides, are given on the left in the bottom panel of the PDOS) of a Au_{25}^{+} cluster. In (A) all orbitals shown have delocalized character except that at −3.86 eV which corresponds to a localized one with atomic d character. Note the shell closure at $n^*=34$, obtained by partial depletion (four electrons) of the number of delocalized electrons, and subsequent single-electron ionization. The cluster is characterized by a spin projection $s_z=3/2$. In (B) we limit ourselves to the top part of the electronic spectrum, and display only two delocalized orbitals, one of 1D character (at −0.99 eV, corresponding to shell closure and opening of the 20-electrons shell-closure gap) and the other of 1F character (at −0.07 eV corresponding to the HOMO−1 energy level near $E-E_F=0$). Orbitals in the energy range $-6.0\ \text{eV} < E\text{-}E_F < -1.5$ eV are of localized atomic d character. The delocalized electrons near −6.19 eV occupy a 1P orbital, and those with energy about −6.95 eV occupy a 1S orbital (not shown). The shell closure at $n^*=20$, is obtained by a five-electron depletion of the number of delocalized electrons by interaction with the protein, and subsequent single-electron ionization. The cluster is characterized by a spin projection $s_z=1$. The weights of the angular momentum components of the displayed KS orbitals are given in S6. For other details see caption of Figure 7.

transforming it to a 34-electron closed-shell superatom structure, characterized by a relatively large (HOMO–LUMO) stabilization gap of close to 0.5 eV (see Figure 5). The same mechanism is operative for the other gold cluster sizes found in the experiments.

Our theoretical discussion presents a novel stabilization mechanism operative in the protein environment that explains the emergence of the particular size sequence of clusters observed in our experiments. The mechanism that we propose differs from the one known to apply for the case of protected gold clusters in solution, involving a large number of protective thiolates (SR) covering the surface of the core gold cluster, for example $Au_{25}(SR)_{18}$, $Au_{38}(SR)_{24}$ and $Au_{102}(SR)_{44}$. In contrast to the latter ones, in our present case only a few cystines (between two and five) are required to bind to the gold cluster to achieve magic number stability—this is consistent with the limited number of cystines in a lysozyme molecule (four cystines per lysozyme). While our studies explain the products formed, the dynamics of cluster formation remains a subject for future experimental and theoretical explorations.

In light of the continuing surge in research activity pertaining to the size-specific properties of gold (as well as other noble metal) clusters in nanotechnology, nanocatalysis, biology and nanomedicine (see, e.g. refs. [1,6,12]), we expect our findings to add to the knowledge base that is imperative for future development, design, and implementation of nanoscale instruments and devices. In particular, recent assessment of research directed at using noble metal (particularly gold) nanoparticles to probe biomolecules and biological processes, as well as for diagnostics and/or regulation and modification of cellular functions, has pointed to a need for detailed knowledge concerning the nature and consequences of interaction between metal nanoparticles and biomolecules, proteins in particular.[13]

© 2013 Wiley-VCH Verlag GmbH & Co. KGaA, Weinheim

Experimental and Theoretical Methods

Materials

Tetrachloroauric acid trihydrate ($HAuCl_4 \cdot 3H_2O$) was prepared in our laboratory starting from pure gold. Lysozyme, extracted from chicken egg white and which had >90% purity, was purchased from Sigma Aldrich. Sinapic acid was also purchased from Sigma Aldrich. All the chemicals were used without further purification. Deionized water was used throughout the experiment.

Synthesis of the Lyz–Au Adduct

Lyz–Au adduct was prepared by the same method as described by Chaudhari et al.[6g] Briefly different concentrations of $HAuCl_4 \cdot 3H_2O$ (1 mM-10 mM) were prepared. To 1 mL 1.5 mM of Lyz, 1 mL of $HAuCl_4 \cdot 3H_2O$ solutions of different concentrations were added and the resultant mixtures were stirred with a magnetic stirrer for 5 min and incubated further for 2 h. The samples were taken out and spotted for MALDI-MS analysis. These were also analyzed by ESI-MS.

Spectrometric Analysis and Instrumentation

MALDI-MS Analysis: Sinapic acid was used as the matrix for MALDI-MS analysis. The matrix solution was prepared using 1:3 acetonitrile:0.1% trifluoroacetic acid in deionized (DI) water. Each time while sampling, 5 μL of the sample was mixed with 100 μL of freshly prepared matrix and sonicated gently for 10 s and then 2.5 μL of the mixture was spotted to yield a dried droplet. An Applied Biosystems Voyager DE Pro MALDI MS instrument was used for the measurements. A pulsed nitrogen laser of 337 nm was used for ionizing the sample. Spectra were collected in the linear positive mode and an average of 250 shots were taken for each spectrum. Measurements were also done in the negative mode, where indicated. In time-of-flight mass spectrometry it is assumed that ions are generated instantaneously upon laser irradiation. The time width for N_2 laser pulse is of the order of a few nanoseconds. When the laser intensity is high enough to exceed the ion generation threshold, ions may continue to be generated even after the completion of laser irradiation. To avoid ion loss, and also to improve resolution, a long delay time of few hundred nanoseconds is typically applied between ion generation and ion extraction. In our study we have used a delay time of 1200 ns to allow the desorbed species to interact in the gas phase.

ESI-MS Analysis: 10 μL of the sample was taken and diluted to 2 mL with DI water. To it 10 μL of trifluoroacetic acid (TFA) (0.1% in DI) was added as ionization enhancer for spectral collection in the positive ion mode. A Thermo Scientific LTQ XL ESI MS instrument was used for this study. Ion spray voltage was kept 4.5 kV and the capillary temperature was set at 250 °C.

Computational Methods

The theoretical results described in this paper have been obtained from calculations using spin density functional theory (SDFT)[14] in conjunction with non-local norm-conserving scalar-relativistic soft pseudopotentials[15] with the valence $5d^{10}$ and $6s^1$ electronic states of the gold atoms (as well as the valence electrons of the atoms of the interacting cysteine molecules: sulfur, oxygen, nitrogen and hydrogen) expanded in a plane-wave basis with a 62 Ry kinetic energy cutoff, and employing the Perdew–Burke–Ernzerhof (PBE) functional in the generalized-gradient approximation (GGA) to the exchange–correlation corrections.[16]

The theoretical explorations of the atomic arrangements and electronic structures of the gold clusters and their interactions with the cystine units of the protein employed the SDFT, using the Born–Oppenheimer (BO) molecular dynamics (MD) method, BO–SDF–MD.[14] This method is particularly suitable for investigations of charged systems since it does not employ a supercell (i.e. no periodic replication of the ionic system is used). Structural optimizations were performed using a conjugate-gradient-like method. For the clusters shown in Figures 7 and 8, we find the following spin projection (s_z) values: Au_{102}^+: $s_z=1/2$; Au_{38}^+: $s_z=3/2$; Au_{25}^+: $s_z=1$. The "partial jellium" picture was first introduced in ref. [2g] and used in the analysis of the electronic structures of bare gold anions. In that paper the expansion in spherical harmonics (see below) was done for each gold atom of the cluster taken as a center. Here we choose to perform the analysis with respect to the center of mass of the cluster.

The projected density of states, $w_{i,l}(R_0)$ were calculated[2g] from the KS orbitals $\psi_i(r+R_{cm})$ corresponding to the KS energy eigenvalue ε_i, where R_{cm} is the center of mass of the cluster (taken from here on as the origin, $R_{cm}=0$), using Equation (4):

$$w_{i,l}(R_0) = \sum_{m=-l}^{l} \int_0^{R0} r^2 dr |\phi_{i,lm}(r)|^2 \tag{4a}$$

$$\phi_{i,lm}(r) = \int d\Omega Y_{lm}(\Omega)\psi_i(r) \tag{4b}$$

Here, Y_{lm} is the spherical harmonic function with angular momentum number l and magnetic quantum number m, and angular momenta up to $l=6$ (l symmetry) are considered. The integration is taken in a sphere of radius R_0, chosen as follows for the three cluster sizes: Au_{102}^+: $R_0=11.6$ Å; Au_{38}^+: $R_0=9.3$ Å; Au_{25}^+: $R_0=8.9$ Å. In plotting the PDOS each $w_{i,l}$ is broadened by a Gaussian of width 0.07 eV.

Acknowledgements

A.B and T.P. thank the Department of Science and Technology, Government of India for continuous support our of research program on nanomaterials. A.B. thanks the Council of Scientific and Industrial Research (CSIR) for a fellowship. The work of B.Y., C.Y. and U.L. was supported by the Office of Basic Energy Sciences of the US Department of Energy under Contract No. FG05-86ER45234 and in part by a grant from the Air Force Office of Scientific Research. Computations were made at the GATECH Center for Computational Materials Science.

Keywords: density functional calculations · electronic states · gold clusters · mass spectrometry · protein–gold adducts

[1] a) *Nanocatalysis* (Eds: U. Heiz, U. Landman), Springer, Berlin **2006**; b) G. C. Bond, C. Louis, D. T. Thompson, *Catalysis by Gold*, Imperial College Press, London, **2006**; c) P. L. Xavier, K. Chaudhari, A. Baksi, T. Pradeep, *Nano Rev.* **2012**, *3*, 14767.

[2] a) C. L. Cleveland, U. Landman, *J. Chem. Phys.* **1991**, *94*, 7376–7396. where some of the nomenclature used in this field was introduced and elaborated on; b) R. L. Whetten, J. T. Khoury, M. M. Alvarez, S. Murthy, I. Vezmar, Z. L. Wang, P. W. Stephens, C. L. Cleveland, W. D. Luedtke, U. Landman, *Adv. Mater.* **1996**, *8*, 428–433; c) C. L. Cleveland, U. Landman, T. G. Schaaff, M. N. Shafigullin, P. W. Stephens, R. L. Whetten, *Phys. Rev. Lett.* **1997**, *79*, 1873–1876; d) H. Häkkinen, R. N. Barnett, U. Landman, *Phys. Rev. Lett.* **1999**, *82*, 3264–3267; e) W. D. Luedtke, U. Landman, *J. Phys. Chem.* **1996**, *100*, 13323–13329; f) X. Xing, B. Yoon, U. Landman, J. H. Parks, *Phys. Rev. B* **2006**, *74*, 165423; g) B. Yoon, P. Koskinen, B.

© 2013 Wiley-VCH Verlag GmbH & Co. KGaA, Weinheim

Huber, O. Kostko, B. von Issendorff, H. Häkkinen, M. Moseler, U. Landman, *ChemPhysChem* **2007**, *8*, 157 – 161.

[3] a) Y. Negishi, K. Nobusada, T. Tsukuda, *J. Am. Chem. Soc.* **2005**, *127*, 5261 – 5270; b) Y. Shichibu, Y. Negishi, T. Tsukuda, T. Teranishi, *J. Am. Chem. Soc.* **2005**, *127*, 13464 – 13465; c) E. S. Shibu, M. A. H. Muhammed, T. Tsukuda, T. Pradeep, *J. Phys. Chem. C* **2008**, *112*, 12168 – 12176; d) M. Zhu, E. Lanni, N. Garg, M. E. Bier, R. Jin, *J. Am. Chem. Soc.* **2008**, *130*, 1138 – 1139; e) M. W. Heaven, A. Dass, P. S. White, K. M. Holt, R. W. Murray, *J. Am. Chem. Soc.* **2008**, *130*, 3754 – 3755; f) M. Zhu, C. M. Aikens, F. J. Hollander, G. C. Schatz, R. Jin, *J. Am. Chem. Soc.* **2008**, *130*, 5883 – 5885; g) Z. Wu, J. Suhan, R. Jin, *J. Mater. Chem.* **2009**, *19*, 622 – 626; h) L. A. Angel, L. T. Majors, A. C. Dharmaratne, A. Dass, *ACS Nano* **2010**, *4*, 4691 – 4700; i) J. Akola, K. A. Kacprzak, O. Lopez-Acevedo, M. Walter, H. Grönbeck, H. Häkkinen, *J. Phys. Chem. C* **2010**, *114*, 15986 – 15987; j) A. C. Dharmaratne, T. Krick, A. Dass, *J. Am. Chem. Soc.* **2009**, *131*, 13604 – 13605; k) C. Zeng, H. Qian, T. Li, G. Li, N. L. Rosi, B. Yoon, R. N. Barnett, R. L. Whetten, U. Landman, R. Jin, *Angew. Chem. Int. Ed.* **2012**, *51*, 13114 – 13118.

[4] a) R. L. Donkers, D. Lee, R. W. Murray, *Langmuir* **2004**, *20*, 1945 – 1952; b) V. L. Jimenez, D. G. Georganopoulou, R. J. White, A. S. Harper, A. J. Mills, D. Lee, R. W. Murray, *Langmuir* **2004**, *20*, 6864 – 6870; c) J. Kim, K. Lema, M. Ukaigwe, D. Lee, *Langmuir* **2007**, *23*, 7853 – 7858; d) Y. Pei, Y. Gao, X. C. Zeng, *J. Am. Chem. Soc.* **2008**, *130*, 7830 – 7832; e) O. Toikkanen, V. Ruiz, G. Rönnholm, N. Kalkkinen, P. Liljeroth, B. M. Quinn, *J. Am. Chem. Soc.* **2008**, *130*, 11049 – 11055; f) H. Qian, M. Zhu, U. N. Andersen, R. Jin, *J. Phys. Chem. A* **2009**, *113*, 4281 – 4284; g) O. Lopez-Acevedo, H. Tsunoyama, T. Tsukuda, H. Häkkinen, C. M. Aikens, *J. Am. Chem. Soc.* **2010**, *132*, 8210 – 8218; h) H. Qian, W. T. Eckenhoff, Y. Zhu, T. Pintauer, R. Jin, *J. Am. Chem. Soc.* **2010**, *132*, 8280 – 8281.

[5] a) P. D. Jadzinsky, G. Calero, C. J. Ackerson, D. A. Bushnell, R. D. Kornberg, *Science* **2007**, *318*, 430 – 433; b) Y.-K. Han, H. Kim, J. Jung, Y. C. Choi, *J. Phys. Chem. C* **2010**, *114*, 7548 – 7552.

[6] a) J. Xie, Y. Zheng, J. Y. Ying, *J. Am. Chem. Soc.* **2009**, *131*, 888 – 889; b) M. A. H. Muhammed, P. K. Verma, S. K. Pal, A. Retnakumari, M. Koyakutty, S. Nair, T. Pradeep, *Chem. Eur. J.* **2010**, *16*, 10103 – 10112; c) A. Mathew, P. R. Sajanlal, T. Pradeep, *J. Mater. Chem.* **2011**, *21*, 11205 – 11212; d) H. Wei, Z. Wang, L. Yang, S. Tian, C. Hou, Y. Lu, *Analyst* **2010**, *135*, 1406 – 1410; e) C.-L. Liu, H.-T. Wu, Y.-H. Hsiao, C.-W. Lai, C.-W. Shih, Y.-K. Peng, K.-C. Tang, H.-W. Chang, Y.-C. Chien, J.-K. Hsiao, J.-T. Cheng, P.-T. Chou, *Angew. Chem.* **2011**, *123*, 7194 – 7198; *Angew. Chem. Int. Ed.* **2011**, *50*, 7056 – 7060; f) P. L. Xavier, K. Chaudhari, P. K. Verma, S. K. Pal, T. Pradeep, *Nanoscale* **2010**, *2*, 2769 – 2776; g) K. Chaudhari, P. L. Xavier, T. Pradeep, *ACS Nano* **2011**, *5*, 8816 – 8827; h) J. S. Mohanty, P. L. Xavier, K. Chaudhari, M. S. Bootharaju, N. Goswami, S. K. Pal, T. Pradeep, *Nanoscale* **2012**, *4*, 4255 – 4262; i) A. Baksi, P. L. Xavier, K. Chaudhari, N. Goswami, S. K. Pal, T. Pradeep, *Nanoscale* **2013**, *5*, 2009 – 2016.

[7] H. W. Kroto, J. R. Heath, S. C. O'Brien, R. F. Curl, R. E. Smalley, *Nature* **1985**, *318*, 162 – 163.

[8] a) J. T. Petty, J. Zheng, N. V. Hud, R. M. Dickson, *J. Am. Chem. Soc.* **2004**, *126*, 5207 – 5212; b) J. Zheng, P. R. Nicovich, R. M. Dickson, *Annu. Rev. Phys. Chem.* **2007**, *58*, 409 – 431.

[9] T. Pradeep, R. G. Cooks, *Int. J. Mass Spectrom. Ion Processes* **1994**, *135*, 243 – 247.

[10] C. F. Shaw in *Gold: Progress in Chemistry, Biochemistry & Technology* (Ed.: H. Schmidbaur), Wiley, New York, **1999**, Chap. 10, pp. 260 – 308.

[11] a) H. Häkkinen, *Chem. Soc. Rev.* **2008**, *37*, 1847 – 1859; b) M. Walter, J. Akola, O. Lopez-Acevedo, P. D. Jadzinsky, G. Calero, C. J. Ackerson, R. L. Whetten, H. Grönbeck, H. Häkkinen, *Proc. Natl. Acad. Sci. USA* **2008**, *105*, 9157 – 9162.

[12] a) M. C. Daniel, D. Astruc, *Chem. Rev.* **2004**, *104*, 293 – 346; b) A. Sanchez, S. Abbet, U. Heiz, W.-D. Schneider, H. Hakkinen, R. N. Barnett, U. Landman, *J. Phys. Chem. A* **1999**, *103*, 9573 – 9578; c) C. Harding, V. Habibpour, S. Kunz, A. N.-S. Farnbacher, U. Heiz, B. Yoon, U. Landman, *J. Am. Chem. Soc.* **2009**, *131*, 538 – 548; d) E. C. Dreaden, A. M. Alkikany, X. Huang, C. J. Murphy, M. A. El-Sayed, *Chem. Soc. Rev.* **2012**, *41*, 2740 – 2779; e) R. R. Arvizo, S. Bhattacharyya, R. A. Kudgus, K. Giri, R. Bhattacharya, P. Mukherjee, *Chem. Soc. Rev.* **2012**, *41*, 2943 – 2970; f) T. L. Doane, C. Burda, *Chem. Soc. Rev.* **2012**, *41*, 2885 – 2911.

[13] a) S. Laera, G. Ceccone, F. Rossi, D. Gilliland, R. Hussain, G. Siligardi, L. Calzolai, *Nano Lett.* **2011**, *11*, 4480 – 4484; b) A. A. Shemetovm, I. Nabiev, A. Sukanova, *ACS Nano* **2012**, *6*, 4585 – 4602; c) S. H. De Paoli Lacerda, J. J. Park, C. Meuse, D. Pristinski, M. L. Becker, A. Karim, J. F. Douglas, *ACS Nano* **2010**, *4*, 365 – 379; d) H. Wei, Z. Wang, J. Zhang, S. House, Y.-G. Gao, L. Yang, H. Robinson, L. H. Tan, H. Xing, C. Hou, I. M. Robertson, J.-M. Zuo, Y. Lu, *Nat. Nanotechnol.* **2011**, *6*, 93 – 97; e) T.-H. Chen, W.-L. Tseng, *Small* **2012**, *8*, 1912 – 1919.

[14] R. N. Barnett, U. Landman, *Phys. Rev. B* **1993**, *48*, 2081 – 2097.

[15] N. Troullier, J. L. Martins, *Phys. Rev. B* **1991**, *43*, 1993 – 2006.

[16] J. P. Perdew, K. Burke, M. Ernzerhof, *Phys. Rev. Lett.* **1996**, *77*, 3865 – 3868.

Received: November 9, 2012
Revised: February 15, 2013
Published online on March 18, 2013

© 2013 Wiley-VCH Verlag GmbH & Co. KGaA, Weinheim